

Air Activation of Glass-Like Carbon Spheres ガラス状炭素球の空気賦活

Michio Inagaki[†] and Tetsuo Nishikawa[†]
稲垣道夫[†], 西川哲男[†]

Abstract Pore development in glass-like carbon spheres with oxidation in dry air was studied through the measurements of oxidation yield, various pore parameters and phenol adsorption. The development of pores was understood by the master curves at 400 °C for oxidation yield, each pore parameters and phenol adsorptivity. The results showed that the conversion between oxidation temperature and time was possible for pore development by air oxidation, *i.e.*, at a temperature between 355 and 430 °C in a flow of dry air. Pore development was supposed to proceed principally the opening of closed pores existed originally in glass-like carbon to form ultramicropores, followed by the collapse and enlargement of ultramicropore to macropore through supermicropore and mesopore.

1. Introduction

Activated carbon has played important roles since pre-historical era and now become even more important materials in various fields of technology. Industrial applications of activated carbons to modern technology, for examples, applications to car canister, the storage of natural gas, the electrode material of electric double layer capacitor, etc., demand strict control of their pore structure¹⁻³. The most important process for the production of these activated carbons is activation, which has been studied by a number of researchers and engineers from different points of view and also different activation processes have been developed, for example, using either steam, ZnCl₂ or KOH in order to develop micropores and to have high surface area⁴⁻⁶. This activation process is the oxidation and gasification of precursor carbons, most of them being hard carbons and containing a large amount of macropores.

One of the authors has been studied the process of gas activation by selecting carbon spheres, which were prepared from phenol resin and had glass-like carbon nanotexture, as the original carbon sample⁷⁻²⁷. In our previous paper¹⁴, the activation process of hard carbon spheres in an atmosphere of wet air at different temperatures and residence times was understood by a master curve for the yield after activation, which suggested the conversion between oxidation temperature and time. On the same carbon spheres, the activation process by dry air was investigated through the measurements of various pore structure parameters, in addition to activation yield^{16,17} and also adsorption behavior for various organics in their aqueous solutions were understood by the master curves for each adsorbates as functions of oxidation temperature and time²³. Also adsorption behavior of methane gas into air-oxidized carbon spheres was studied²⁰.

In the present paper, pore development in carbon spheres in an atmosphere of dry air was discussed through master curves for each pore parameters^{16,17}.

2. Materials and Characterization Techniques

2.1 Materials

Carbon spheres prepared from a resol-type phenol resin spheres by carbonization at 1000 °C were selected, which had the particle size of ca. 10 μm. Carbon spheres of 10.0 g were placed in an alumina boat (50 x 90 mm and 10 mm deep) and heated at different temperatures between 355 and 430 °C for different periods from 1 to 100 h in a flow of dry air in a tubular furnace (60 mm in inner diameter). The air was dried by passing through a silica gel column and then passing on the surface of P₂O₅ with a flowing rate of 50 mL/min.

After air oxidation, oxidation yield was calculated from the mass loss during oxidation process.

2.2 Pore structure characterization

On carbon spheres thus oxidized, adsorption/desorption isotherm of N₂ was measured at 77 K. From the isotherm measured, different pore parameters were determined using different analytical methods. BET surface area was calculated using adsorption data up to the relative pressure P/P₀ less than 0.3. Through the analysis by so-called α_s plot, total surface area, external surface area and micropore volume were calculated, and microporous surface area was derived as a balance between total and external surface areas. Based on DFT analysis, pore size distribution in the size range corresponding to micropores (up to 2 nm) was determined. From the cumulation, the volume of micropores (< 2.0 nm) and also that of ultramicropores (< 0.8 nm) were obtained. The volume of mesopores (2 ~ 50 nm) was determined by using BJH method. SEM observation on the surface of carbon spheres was performed under the electron beam accelerated by 10 kV.

Adsorption of phenol from its aqueous solution was determined on the carbon spheres oxidized. The saturated amount of phenol adsorbed into carbon spheres was determined after keeping the sample spheres in the phenol solution with a concentration of 0.02 mol/L for 24 h under stirring at room temperature.

In order to understand the mechanism of micropore formation in the very beginning of oxidation, the

[†]愛知工業大学工学部応用化学科(豊田市)
Faculty of Engineering, Aichi Institute of Technology

measurement of small angle X-ray scattering (SAXS) was carried out for carbon spheres slightly oxidized. Details of experimental conditions were reported in our paper¹⁷⁾. The fundamentals on these techniques have to be referred the respective original papers²⁷⁻²⁹⁾.

3. Air Activation Process

-Master Curve and Apparent Activation Energy

3.1 Oxidation yield

Oxidation yield is plotted against oxidation time for different oxidation temperatures in Fig. 1a. Master curve at

a reference temperature of 400 °C for the oxidation in the present activation condition (dry air with a flow rate of 50 mL/min) was possible to be obtained by shifting the experimental points at each oxidation temperature along the abscissa (logarithm of oxidation time) to be consistent with the points measured at 400 °C (Fig. 1b).

Plot of shift factors against the inverse of oxidation temperature (Arrhenius plot) gave a linear relation, as shown in Fig. 1c, and its slope gave an apparent activation energy ΔE of about 150 kJ/mol. In wet air, ΔE of about 200 kJ/mol was obtained, as reported in our previous paper¹⁴⁾.

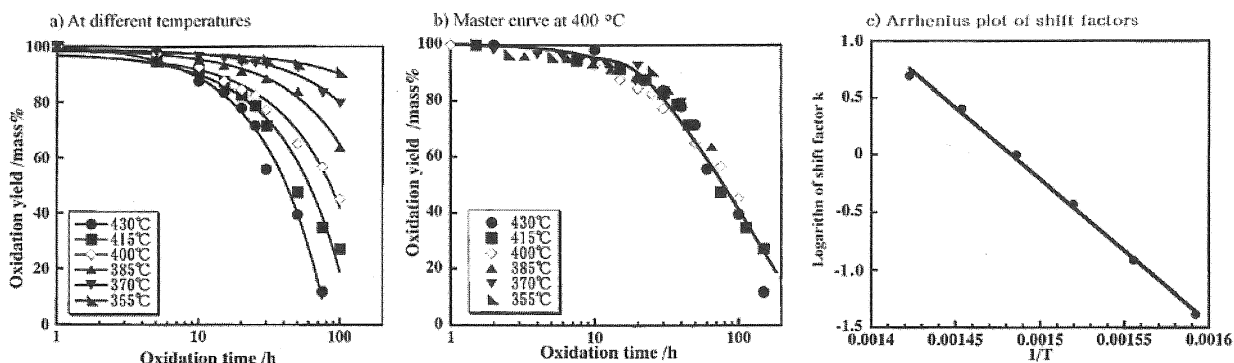


Fig. 1 Oxidation yield as functions of oxidation temperature and time.

3.2 BET surface area

BET surface area was plotted as functions of oxidation temperature and time in Fig. 2a. BET surface area obtained at 355 °C increased slightly from about 400 m²/g with increasing oxidation time. At the highest temperature of 430 °C, BET surface area quickly increased after 30 h oxidation but then decreased with increasing oxidation time. However, it has to be pointed out that BET surface area was

already a high value close to 600 m²/g even after 10 h oxidation at 400 °C. Intermediate oxidation temperatures resulted in intermediate change in BET surface area, as shown by dotted line for 400 °C in the figure. The same procedure as oxidation yield was applied to obtain the master curve at 400 °C for BET surface area (Fig. 2b). To construct this master curve, the same values of shift factors as those used for oxidation yield were applied.

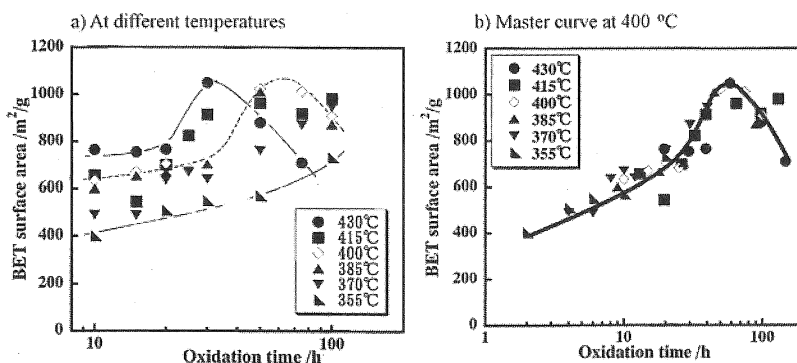


Fig. 2 BET surface area as functions of oxidation temperature and time

Even though there are some scattering of experimental points, the master curve was able to be obtained using the same shifting procedure as oxidation yield, in other words, conversion between oxidation temperature and time was possible for BET surface area. BET surface area increased gradually in the beginning of oxidation, followed by relatively rapid increase. However, further oxidation

yielded rapid decrease in BET surface area.

By the present simple oxidation in dry air, BET surface area above 1000 m²/g could be obtained by selecting appropriate conditions, about 30 h at 430 °C or about 65 h at 400 °C.

3.3 α_s plot analysis

Four pore parameters, micropore volume, microporous surface area, external surface area and total surface area, which were determined by α_s plot analysis, were shown as master curves at 400 °C in Figs. 3a to 3d, respectively. To construct these master curves, the same shift factors at each oxidation temperature as those for oxidation yield were used.

Micropore volume and microporous surface area showed a maximum, but external surface area started to increase around 10 h oxidation and continued to increase by further oxidation, the former was much larger, by about one order of magnitude, than the latter in the present samples. Total surface area showed a maximum, α_s BET surface area

did, because this is the sum of microporous and external surface areas.

The master curves on micropores, *i.e.*, micropore volume (Fig. 3a) and microporous surface area (Fig. 3b), reveal the formation of a large amount of micropores by the oxidation at 400 °C only 1.5 h, giving about 0.2 ml/g of micropore volume and about 400 m²/g of microporous surface area. This experimental fact is due to the opening of the closed pores which exist in the original glass-like carbon, as will be shown in the following section 4.

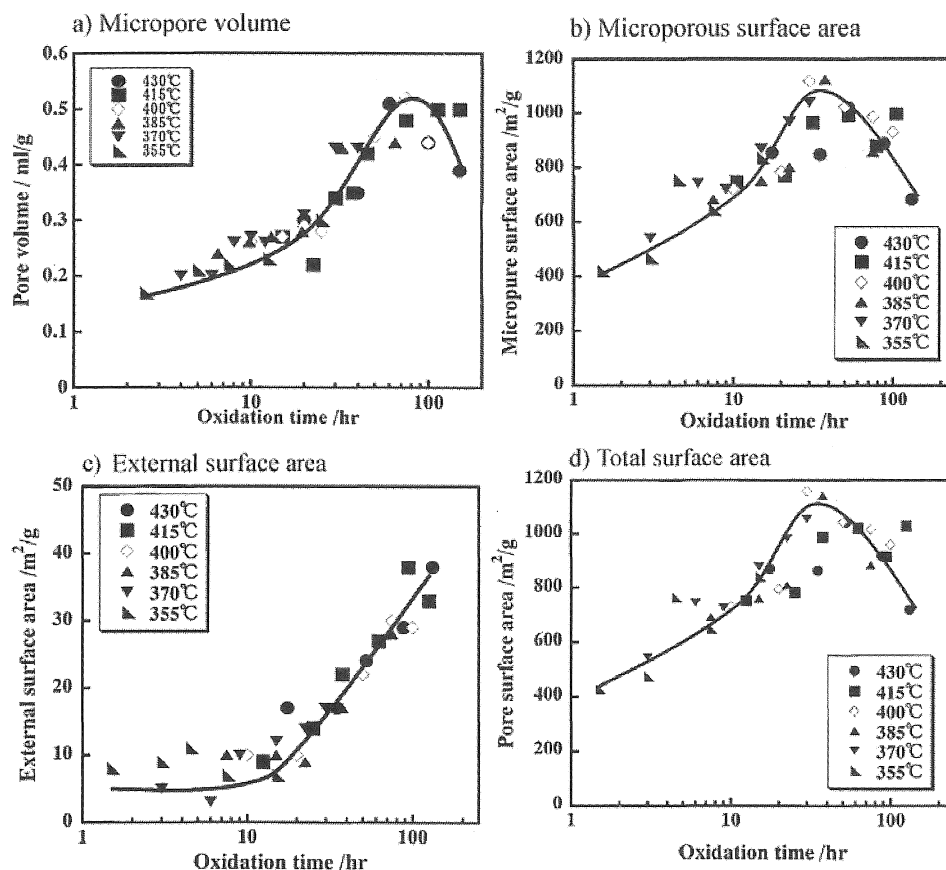


Fig. 3 Master curves for different pore parameters obtained by α_s plot analysis.

3.4 DFT and BJH analyses

On the same samples pore size distributions in micropores ranging from 0.4 to 2 nm and mesopores from 2 to 50 nm was determined by using DFT and BJH methods, respectively. From the cumulative pore volumes of respective method, micropore and mesopore volumes were calculated for each samples and plotted as functions of oxidation temperature and time. As we did for oxidation yield, BET surface area and four pore parameters, the master curves at 400 °C for micropore and mesopores volumes were obtained, as shown in Fig. 4. Micropore volume was separated into two subclasses, ultramicropore and supermicropore, as shown only master curves for each parameter in Fig. 4a. On the pore size distribution determined by BJH method, the pores with the size of above

5 nm size were negligibly small amount.

In the beginning of oxidation, micropore volume increased gradually with increasing oxidation time, which were supposed to be due to the increase in ultramicropore volume. Beyond 10 h oxidation, micropore volume increased rapidly, where ultramicropores decreased gradually and supermicropores increased, no development of mesopores above 2 nm yet. Beyond 30 h oxidation, mesopores seemed to be developed, though the development of supermicropores was still continued. After 50 h oxidation, however, micropore volume decreased rapidly with increasing oxidation time (Fig. 4a), as microporous surface area did (Fig. 3b), but mesopore volume continued to increase (Fig. 4b), as external surface area did (Fig. 3c).

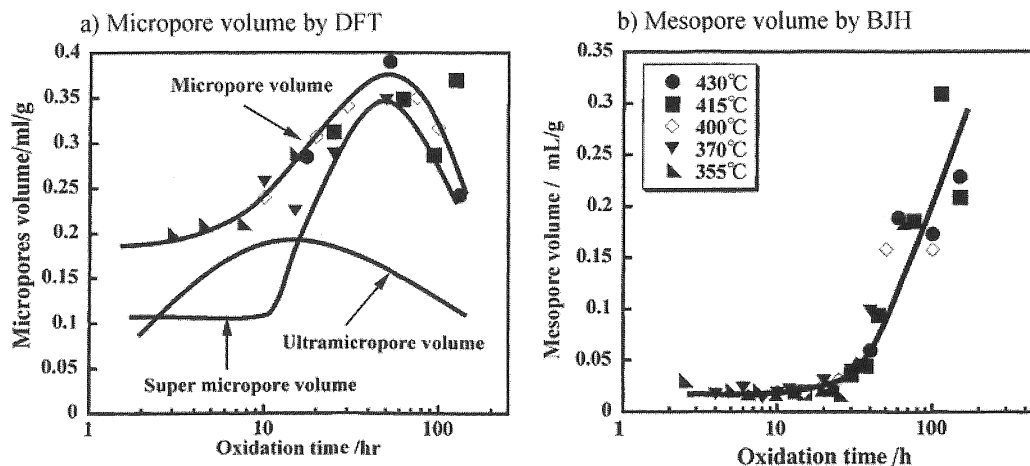


Fig. 4 Master curves for micropores and mesopores.

4. Formation Mechanism of Micropores

In Fig. 5a, adsorption/desorption isotherm of N_2 gas at 77 K is shown for the carbon spheres oxidized for 2.5, 20 and 75 h at 400 °C, each of which corresponds to the beginning of pore development, that of increasing micropore volume and that at the maximum in micropore volume, respectively, as shown together with the isotherm for the original carbon spheres in Fig. 4a. Adsorption of N_2 gas became marked by the oxidation at 400 °C for 2.5 h, with a pronounced

difference from the original spheres. This increase in adsorption was resulted from the increases in BET surface area from few to about 400 m^2/g and in micropore volume measured by α_s plot from almost zero to about 0.17 ml/g, as shown in Fig. 2a and 3a, respectively. With increasing oxidation time at 400 °C, the adsorbed amount of N_2 gas increased and the isotherms observed change from Type I to Type II, suggesting the increase in macropores from micropore dominant solid.

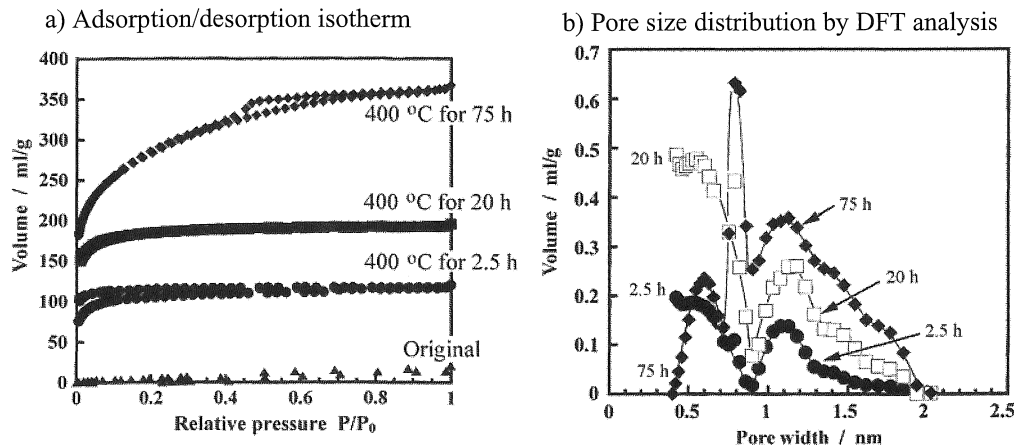


Fig. 5 Adsorption/desorption isotherms and pore size distributions for carbon spheres oxidized.

Pore size distributions measured by DFT analysis on the oxidized carbon spheres are shown in Fig. 5b. On the carbon spheres oxidized at 400 °C for 2.5 h, pores less than 0.4 nm seemed to be predominant, even though these pores could not be measured, in other words, most of the pores existed originally in the carbon spheres were not yet opened and only the entrances having the size less than 0.4 nm were formed. After 20 h oxidation at 400 °C, the population of the pores (openings of pores) with the size of around 0.6 and 1.2 nm increased and the total micropore volume increased from about 0.17 ml/g to about 0.28 ml/g (Fig. 4a). The pore size distribution curve observed on the sample oxidized at 400 °C for 20 h suggested a high population of the pores

smaller than 0.4 nm, higher than the samples oxidized for 2.5 h, suggesting that all pores originally existed in carbon sphere were not yet opened. By the oxidation for 75 h, the population of the pores smaller than 0.4 nm became almost zero, in other words, all closed pores were opened, and that of the pores with the size of around 0.6 nm decreased, but that of the pores with 1.2 nm size increased markedly. On this sample, the presence of the pores with the size of about 0.9 nm was clearly observed. In the case of the sample oxidized for 20 h, there was also small population of the pores with almost the same size.

At 400 °C, the trend to increase the volume of pores with the sizes of around 0.6 and 1.2 nm was clearly observed,

and the pores less than 0.4 nm seems to decrease. At 430 °C, the same trend could be recognized. After 75 h oxidation at 430 °C (150 h at 400 °C), however, pore volume corresponding to the pores with 0.6 and 1.2 nm sizes decreased, probably because pores were widened to more than 2 nm by oxidation.

The results shown in Fig. 5b suggested the gradual change in pore size (the sizes of openings) from less than 0.4 nm to 0.6 nm and then to 1.2 nm. The same analysis by DFT method on the samples oxidized at intermediate conditions, *i.e.*, oxidation time from 2.5 to 75 h at 400 °C, was supported this supposition based on Fig. 5b. On the samples oxidized for more than 75 h at 400 °C, a rapid decrease in micropore volume and a corresponding rapid increase in mesopore volume was observed in Fig. 4.

In Fig. 6a, pore width determined from SAXS analysis was plotted as functions of oxidation temperature and time.

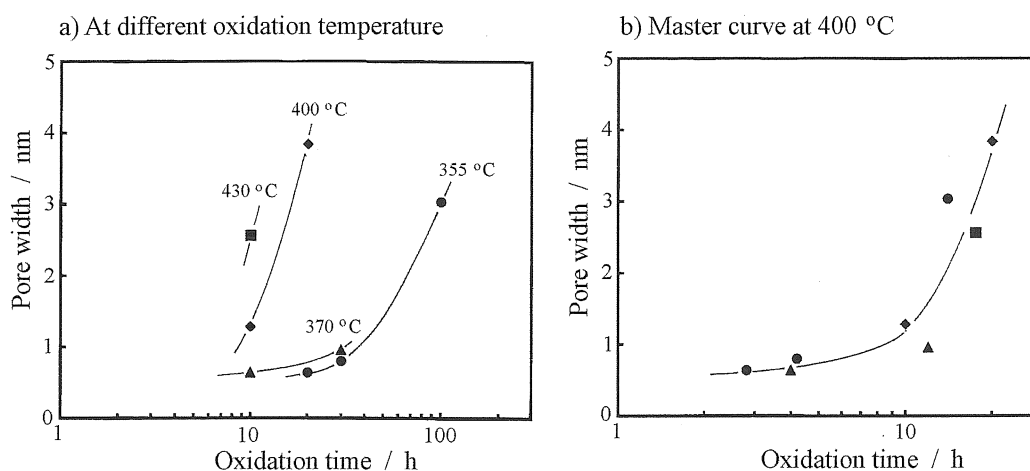


Fig. 6 Micropore width determined through SAXS analysis as functions of oxidation temperature and time.

The micropores formed in the carbon spheres had the average size of 0.7–0.8 nm by the air oxidation at 400 °C for 2.5 h, grew slightly to about 1.0 nm after 10 h oxidation and then increased rapidly with increasing oxidation time. The pore size thus determined by SAXS analysis shows a good correspondence to that observed by gas adsorption with DFT analysis (Fig. 5b). Therefore, the pores detected by SAXS are supposed to be the holes (openings) formed on the wall of pores originally existed in carbon sphere. This supposition seems to be consistent with the result that pore size increases very rapidly (Fig. 6b).

The present results obtained by N₂ gas adsorption and SAXS may suggest that the principal process for the formation of micropores was the opening of the closed pores, which existed originally in the carbon spheres.

5. Adsorption of phenol

Adsorption of phenol from its aqueous solution was saturated after 10 h, as an isotherm for the carbon spheres oxidized at 400 °C for 100 h was shown in Fig. 7a. For carbon spheres oxidized, therefore, the saturated amount of phenol adsorbed was calculated from the concentration change after being kept for 24 h and plotted as functions of oxidation temperature and time in Fig. 7b. By the same

The pore width calculated was obtained by subtracting the contribution from the spaces among spheres and also closed pores existed in the original spheres, and so it was reasonably supposed to the average size of pores formed by oxidation. The pore width measured increases rapidly with increasing oxidation time at each oxidation temperature. The higher oxidation temperature gives the increase in pore width with the shorter oxidation time, although the measurements were restricted to the beginning of oxidation in order to discuss on the formation of micropores. The experimental points measured at different temperatures could be shifted along the abscissa, oxidation time in the logarithmic scale, to deduce the master curve at 400 °C (Fig. 6b). The shift factors for each oxidation temperature were exactly the same as those used for oxidation yield in Fig. 1c. The master curve for micropore width determined through SAXS analysis was also obtained, as for different pore parameters.

procedure with the same shift factors as those for oxidation yield, the master curve for phenol adsorption for the carbon spheres oxidized at 400 °C was obtained, as shown in Fig. 7c.

In order to understand the correspondence between adsorptivity for phenol (saturated amount of phenol adsorbed) and pore structure of the oxidized carbon spheres, adsorptivity measured was plotted against micropore volume obtained from α_s plot. As shown in Fig. 8a, no correspondence between these two parameters was observed. However, a good linear relation was obtained between adsorptivity and the volume for ultramicropores, as shown in Fig. 8b.

If the attention was paid to two special points indicated by *1 and *2 in Fig. 8a, which were obtained on the carbon spheres oxidized at 430 °C for 10 and 75 h, respectively, micropore volume for these two spheres was not so much different, but their adsorptivity for phenol was quite different. The former contained a large amount of ultramicropores but in the latter only a small amount of ultramicropores was remained after long time oxidation, as shown in Fig. 8b, which resulted in a big difference in adsorptivity for phenol. Adsorptivity values for these two points *1 and *2 are on the straight line plotted against ultramicropore volume (Fig. 8b).

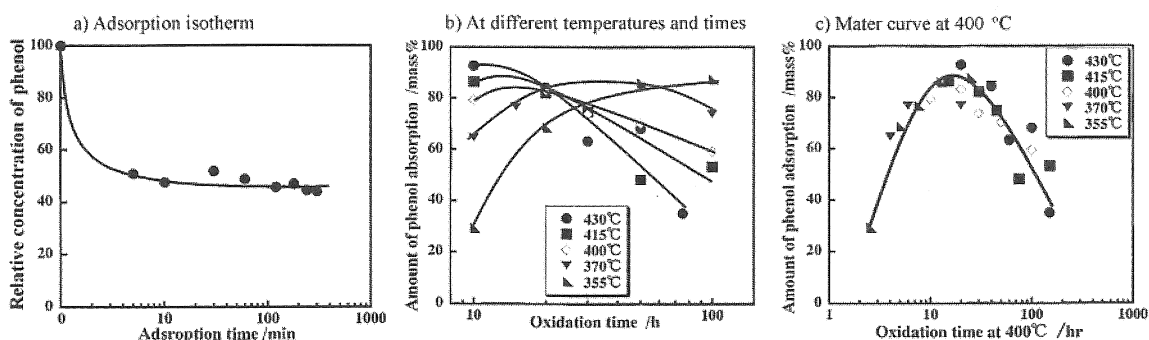


Fig. 7 Adsorption of phenol from its aqueous solution.

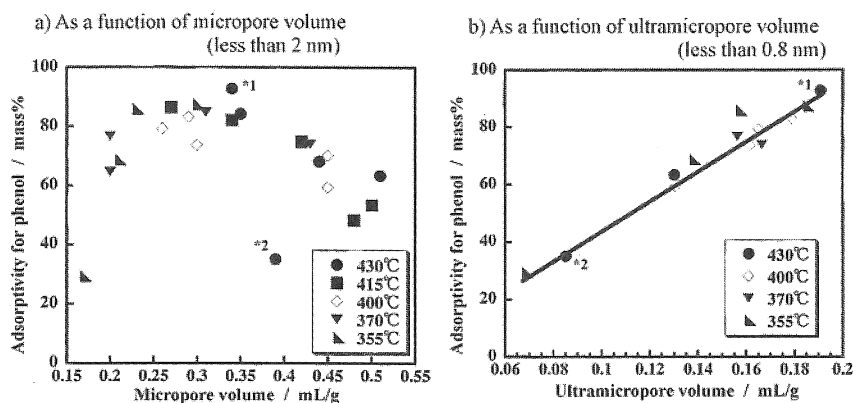


Fig. 8 Relation of phenol adsorptivity on micropore volume.

6. Discussion

The shift factors used in order to construct master curves for not only oxidation yield but also various pore parameters and adsorptivity for phenol gave the apparent activation energy of about 150 kJ/mol. If we take into account of the fact that the formation energies of CO_2 and CO gases are about 394 and 111 kJ/mol, respectively, the obtained value of apparent activation energy is in between these two formation energies. In wet air, the apparent activation energy of about 200 kJ/mol was obtained¹⁴⁾. The activation energy determined here is only apparent value, in other words, alternative expression of the conversion factors between temperature and time for oxidation. In the present work, therefore, the discussion to compare the present activation energy values with those reported on the basis on the kinetic studies of oxidation and gasification of various carbon materials was not carried out. The value of activation energy obtained by the present shifting procedure is supposed to depend on the particle size and morphology, as well as oxidation conditions, such as oxidizing agent and its concentration and flow rate, etc.

It has to be pointed out here that the comparison among the absolute values of pore parameters, which were determined by different methods of analysis, was difficult

because these methods were based on the different assumptions. However, relative changes in various pore parameters with time at a reference temperature are possible to be compared using the master curves with each other. The master curve of BET surface area (Fig. 2b) is very similar with that of microporous surface area determined by α_s plot (Fig. 3b), which is reasonable because BET surface area is governed by the presence of micropores. The former gave the maximum at about 65 h oxidation at 400 °C, but the latter at about 30 h oxidation, shifting to shorter oxidation time, which is reasonable by taking into a consideration that mesopores are also contribute to BET surface area. The development of mesopores started from about 30 h oxidation (Fig. 4b). External surface area measured by α_s plot (Fig. 3c) has very similar change with oxidation time to that of mesopore volume (Fig. 4b). The master curves of micropore volume determined by α_s plot and DFT method (Fig. 3a and 4a, respectively) are also similar with each other to show a maximum as those for microporous surface area (Fig. 3b) and BET surface area (Fig. 2b). Maxima observed on BET, total and microporous surface area (Fig. 2b, Fig. 3d and Fig. 3b, respectively), are reasonably understood as a result of the competition between enlargement and collapse of pores and subsequent pore surface area loss.

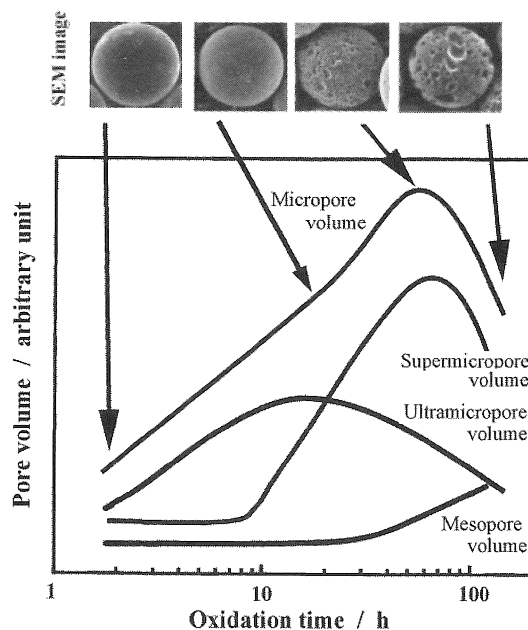


Fig. 9 Development of pores in carbon spheres through air oxidation.

In Fig. 9, master curves for micropore volume determined by α_s plot, ultramicropore and supermicropore volumes by DFT method and mesopore volume by BJH method are reproduced in order to make the comparison easier, together with some SEM images to show the appearance of sphere. In the beginning of oxidation, *i.e.*, up to 10 h oxidation at 400 °C, the main process is the formation of ultramicropore, mainly due to opening of closed pores existed originally in glass-like carbon nanotexture. Above 10 h up to about 60 h, relative amount of ultramicropores formed decreased but supermicropores increase with increasing oxidation time. Above 65 h, micropores (a sum of ultra- and super-micropores) decreased rapidly but mesopore volume increased slightly, which resulted in the decrease in surface areas measured by different methods. This change in pore volumes may suggest the opening of closed pores to form ultramicropores, followed by the gradual enlargement and collapse of pores from ultramicropore to macropore through supermicropore and mesopore.

SEM observation of sphere surface seems to agree with this pore development sequence, as shown in Fig. 9, and it gives some information on macropores, which could not be measured through the gas adsorption analyses. After few hours oxidation, no change on the surface of sphere was detected because micropores could not be seen under SEM. After around 20 h oxidation only few pit-like holes were observed, where supermicropores and mesopores were supposed to be developed. Around and after passing through the maximum of micropore volume, the surface of spheres became rough due to the formation of macropores on the surface.

To understand the oxidation reactions from the view point of gasification, it was proposed to normalize the fractional burn-off in different atmospheres (different oxidizing agents, such as O₂, steam and CO₂, and their different pressures) as a function of $t/t_{0.5}$, where $t_{0.5}$ is the time giving fractional burn-off of 0.5²⁸⁾. The experimental

data of burn-off obtained at a constant temperature for each oxidizing agent were successfully unified to one curve. This analysis procedure was used for the analysis of gasification reaction of chars^{29,30)}, and also successfully applied to the data measured at different temperatures³¹⁾ to get so-called "unification curves".

Unification curves obtained are expressed as a function of dimensionless time $t/t_{0.5}$, but master curves derived in the present work are expressed by real time at a reference temperature. The former seems to be useful to compare the gasification of various carbonaceous materials and to discuss its mechanism, but the latter may useful to discuss the activation conditions to prepare activated carbons.

7. Conclusion

Pores were developed in carbon spheres by the oxidation in dry air. The development of pores was understood by the master curves for each pore parameters, in other words, the conversion between oxidation temperature and time was possible for pore development for the oxidation at a temperature between 355 and 430 °C in a flow of dry air. Pore development was supposed to be proceeded principally the opening of closed pores existed originally in glass-like carbon nanotexture to form ultramicropores, followed by the collapse and enlargement of ultramicropore to macropore through supermicropore and mesopore.

Acknowledgement

The present work was partly supported by a grant of the Frontier Research Project "Materials for the 21st Century -Materials Development for Environment, Energy and Information-" from Ministry of Education, Culture, Sports, Science and Technology. The authors would like to express their sincere thanks to Profs. K. Nishikawa of Chiba

University, K. Oshida of Nagano National College of Technology and K. Fukuyama of Meiji Gakuin University and Dr. K. Hatakeyama of Chiba University for their cooperation and encouragement.

References

- 1 T.D. Burchell, Ed. (1999) *Carbon Materials for Advanced Technologies*, Pergamon.
- 2 M. Inagaki (2000) *New Carbons -Control in structure and functions-*, Elsevier.
- 3 M. Inagaki and F. Kang (2006) *Carbon Materials Science and Engineering - From Fundamentals to Applications-*, Tsinghua Univ. Press.
- 4 Y. Sanada, M. Suzuki, K. Fujimoto, Ed. (1992) *Activated Carbons -Fundamentals and Applications-*, Kodansha Sci.
- 5 F. Rodrigez-Reinoso, *Introduction to Carbon Technologies*, Marsh H, Heintz EA, F.Rodriguez-Reinoso Ed., Univ. de Alicante, p. 35-101 (1997).
- 6 F. Derbyshire, M. Jagtoyen, M. Thwaites. *Activated Carbons - Production and Application*. In: J.W. Patrick Ed., Porosity in Carbons, Edward Arnold (1995) 227-252.
- 7 M. Inagaki and M. Nakashima, *Tanso*, **1994** [No.162] 61-65 (1994).
- 8 M. Inagaki and M. Sunahara, *Tanso*, **1998**[No.183] 146-150 (1998).
- 9 M.I. Kim, C.H. Yun, Y.J. Kim, C.R. Park and M. Inagaki, *Carbon*, **40**, 2003-2012 (2002).
- 10 M.Inagaki, M.Sunahara A.Shindo, V.Vignal and H.Konno, *J.Mater.Res.*, **14**, 3208-3210 (1999).
- 11 V. Vignal, A. Morawski, H. Konno and M. Inagaki, *J. Mater. Res.*, **14**, 1102-1112 (1999).
- 12 M. Inagaki, V. Vignal, H. Konno and A. Morawski, *J. Mater. Res.*, **14**, 3152-3157 (1999).
- 13 M. Inagaki, E. Bourelle, V. Vignal, H. Konno, A.W. Morawski, *Synth. Met.*, **125**, 231-238 (2002).
- 14 M. Inagaki and T. Suwa, *Mol. Cryst. Liq. Cryst.* **386**, 197 (2002)
- 15 Y. J. Kim, M. I. Kim, C. H. Yun, J. Y. Chang, C. R. Park and M. Inagaki, *J. Colloid Interface Sci.* **274**, 555-562 (2004)
- 16 T. Nishikawa and M. Inagaki, *Ads. Sci. Tech.* **23**, 827-837 (2005).
- 17 M. Inagaki, T. Nishikawa, K. Oshida, K. Fukuyama, Y. Hatakeyama and K. Nishikawa, *Ads. Sci. Tech.*, **24**, 55-64 (2006)
- 18 M. Inagaki and M. Nakashima, *Carbon*, **30** 1135-1136 (1992).
- 19 M. Nakashima, S. Shimada, M. Inagaki and T. A. Centeno, *Carbon*, **33**, 1301-1306 (1995).
- 20 O. Tanaike, M. Fukuoka and M. Inagaki, *Synth. Met.*, **125**, 255-257 (2002).
- 21 A. W. Morawski and M. Inagaki, *Desalination*, **114** 23-27 (1997).
- 22 A.W. Morawski, R. Kalenczuk and M. Inagaki, *Desalination*, **130**, 107-112 (2000).
- 23 M. Inagaki and M. Sakanishi, *Adsorption Sci. Tech.*, **21**, 587-595 (2003).
- 24 M. Toyoda, Y. Nanbu, T. Kito, M. Hirano and M. Inagaki, *Desalination*, **159**, 273-282 (2003).
- 25 J. M. Skowronski and M. Inagaki, *Karbo*, **2002**, 8-11 (2002).
- 26 L. Wang, M. Fujita and M. Inagaki, *Electrochimica Acta*, **51**, 4096-4102 (2006)
- 27 L. Wang and M. Inagaki, *New Carbon Mater.* (in press).
- 28 O. M. P. Mahajan, R. Yarzab, P. L. Walker Jr., *Fuel*, **57**, 643 (1978).
- 29 S. Kasaoka, Y. Sakata, and C. Tong, *Intl. Chem. Eng.*, **25**, 160 (1985).
- 30 F. F. Peng, I. C. Lee, R. Y. K. Yang, *Proc. 3rd Pittsburgh Coal Conf.*, p. 730. (1986)
- 31 K. Raghumathan, R. Y. K. Yang, *Ind. Eng. Chem. Res.*, **28**, 518 (1989).